Direct reduction of iron oxides based on steam reforming of bio-oil: a highly efficient approach for production of DRI from bio-oil and iron ores

Feiyan Gong,[a] Tongqi Ye,[a] Lixia Yuan,[a] Tao Kan,[a] Youshifumi Torimoto,[b] Mitsuo Yamamoto[c] and Quanxin Li*[a]

Received 3rd August 2009, Accepted 30th September 2009
First published as an Advance Article on the web 30th October 2009
DOI: 10.1039/b915830h

Production of direct reduced iron (DRI) was performed by a novel and environmentally friendly approach through a systematic experimental process development and process integration study on bio-oil reforming and iron ores reduction. The Ni–Cu–Zn–Al_2O_3 catalyst is one of most suitable candidates for bio-oil reforming because this non-noble metal catalyst can efficiently reform the bio-oil to H_2 and CO_2 at a lower operating temperature (450–500 °C) with a longer lifetime. The catalytic activities of the Ni–Cu–Zn–Al_2O_3 catalyst for different processes, including the reforming of the oxygenated organic compounds in the bio-oil, the water–gas shift reaction and the decomposition of organic compounds, have been investigated. A hydrogen yield of 87.4% with a carbon conversion of 91.8% was obtained at $T = 500$ °C and S/C = 6.1. The hydrogen content reached about 94.6 vol% after simple purification by removing CO_2. Furthermore, direct reduction of iron oxides at different reduction temperatures was investigated using on-line rich-hydrogen reducing gases. The metallization for production of DRI from three ore powders (limonite, hematite and magnetite) and hematite pellets ranges from 93 to 97% at 850 °C for 1 h reduction. The reduction process from the oxidized iron to metallic iron and the intermediate phases were investigated *via* chemical analysis, X-ray diffraction and X-ray fluorescence analyses. The green DRI process with high reduction efficiency and real environmental benefits would, potentially, be a useful route to produce DRI from bio-oil or biomass.

1. Introduction

With increasing concerns about special steel demand, global climate change, and the growing restriction of coke as a reducing agent, there has been an increased interest in the implementation of new iron-making approaches (*e.g.*, using direct reduced iron (DRI) to produce special steel).[1–5] Direct reduction processes are considered to be the most promising alternative iron-making route and have achieved commercial applicability to some extent in various technologies.[6–8] According to the raw materials, there are two main technologies used for production of DRI, *i.e.*, the natural gas-based and coal-based processes.[4,7,9–11] The gas-based processes, such as Midrex and HYL, are relatively proven technologies with a present market share of 75% for direct reduced iron (DRI) production.[1,6,12,13] Since these processes can only be used where natural gas is relatively inexpensive, a family of coal-based DRI processes have also been developed.[4,9] However, natural gas and high-grade coal are concentrated in only a few regions of the globe, and their reserves are declining. In view of growing environmental concerns and the depletion of fossil sources, development of a "green" DRI technology is needed using alternative energy sources such as biomass. Lignocellulosic biomass has attracted considerable attention in recent years as an alternative energy source feedstock or for production of other industrial products, because it is a rich, environmentally friendly and renewable resource which is globally available.[14–17] Only a small part of biomass is currently used for power generation and production of bio-fuels such as bio-ethanol or bio-diesel *etc*.[18,19] Further research and development to produce high value-added products using biomass, with a competitive cost compared to fossil sources-based routes, is definitely required.

Hydrogen is an important raw material for the chemical industry and it is a potentially clean fuel which could have an important role in reducing greenhouse gas emissions for the future.[20,21] Direct reduction of iron ores with H_2 as the reducing agent could have several advantages such as high reduction efficiency, low carbon content in the product and decreased release of CO_2.[22–26] Currently, commercially-used hydrogen is mainly produced on a large scale by steam reforming of natural gas,[27] together with the supplementary processes of catalytic steam reforming oil-derived naphtha, partial oxidation of heavy oils, and gasification of coal, as well as electrolysis of water.[28–32] However, hydrogen production from fossil sources will increase environmental problems such as global warming and local pollution.[33,34] On the other hand, using H_2 doped with H_2S (*e.g.*, derived from coal) as a reducing atmosphere for the reduction of iron oxides will cause residual sulfur problems, which

[a]*Department of Chemical Physics, Lab of Biomass Clean Energy, University of Science & Technology of China, Hefei, Anhui, 230026, P.R. China. E-mail: liqx@ustc.edu.cn*
[b]*Oxy Japan Corporation, 7th Floor, Miya Building, 4-3-4, Kojimachi, Chiyoda-ku, Tokyo, 102-0083, Japan*
[c]*College of Arts and Sciences, The University of Tokyo, 3-8-1 Komaba, Meguro-ku, 153-8902, Japan*

have a detrimental effect on powder metallurgy applications.[24] Recently, the production of hydrogen using biomass as an alternative feedstock has attracted considerable attention.[14,16,35]

Bio-oil, derived from biomass *via* a fast pyrolysis process, generally contains numerous and complex oxygenated organic compounds including acids, alcohols, aldehydes, ketones, substituted phenolics and other oxygenates derived from biomass carbohydrates and lignin.[27,36,37] Bio-oil represents another potential source of renewable chemicals, which can be readily stored and transported.[27,36,38] The steam reforming of bio-oil involves fast pyrolysis of biomass to generate bio-oil which then undergoes reforming to produce a gaseous rich-hydrogen mixture.[16,36,39]. Producing hydrogen through bio-oil reforming is probably one of the most promising options because it can achieve high hydrogen yield and high hydrogen content. The steam reforming of the bio-oil would be mainly determined by the ability of a catalyst to catalyze the steam reforming reactions of the oxygenated organic compounds ($C_nH_mO_k$) in bio-oil ($C_nH_mO_k + (n-k)\,H_2O = nCO + (n-k+m/2)\,H_2$), and the water-shift reaction ($CO + H_2O \rightarrow CO_2 + H_2$).[39,40] In the case of the high temperature reforming of bio-oil, partial thermal decomposition of bio-oil and the Boudouard reaction ($2CO \rightarrow CO_2 + C$) may occur simultaneously. Although substantial research work on the stream reforming of hydrocarbons (*e.g.*, CH_4) and single oxygenated organic compounds (*e.g.*, methanol, ethanol, acetic acid *etc.*) has been extensively carried out and well reviewed in the past,[41–43] systematic studies on bio-oil reforming and its practicability are very limited. Two main problems—exorbitant reforming temperatures and catalyst deactivation—remain serious challenges in the production of hydrogen from bio-oil.[44–49] In contrast to the reforming process for a single organic compound, bio-oil reforming seems quite different, at least in following three respects: firstly, the reforming temperature required to achieve an efficient conversion of bio-oil for a given catalyst is, generally, much higher than that of a single oxygenated organic compound. For example, a nearly complete conversion of ethanol (about 98%)[42] and a 42% conversion of acetic acid[43] can be obtained at 400 °C using the 18wt% NiO/Al_2O_3 catalyst. However, the carbon conversion of bio-oil using the same catalyst was very low (about 14.7%) at 400 °C, and even at 600 °C only reached 65.4%.[49] Higher operating temperatures for bio-oil reforming may be attributed to the fact that the bio-oil contains a large amount of lower reforming active compounds such as phenolics and ketones *etc.*. In addition, the product distribution from bio-oil reforming is also quite different from single oxygenated organic compound such as ethanol and acetic acid.[42,43,49] Secondly, catalyst inactivity in bio-oil reforming is, generally, much more serious than in the reforming process of single oxygenated organic compounds.[42,43,47–49] Generally, catalyst deactivation is mainly caused by the deposition of carbon (coke formation) on the catalyst. No serious deposition of carbon occurs in ethanol reforming using the NiO/Al_2O_3 catalyst,[42] but a notable amount of carbon deposition was observed in bio-oil reforming.[42,43,47–49] Thirdly, the reaction channels in bio-oil reforming should be much more complex than those in the reforming process of single organic compounds because the bio-oil contains multiple types of organic compounds and a lot of reaction channels and intermediates may occur in bio-oil reforming. Accordingly, the development of non-noble metal catalysts suitable for bio-oil reforming, optimization of the reforming conditions, and knowledge of the reaction mechanism and catalyst inactivation processes are required.

In our previous work, attention has been paid to the fast pyrolysis of biomass, the gasification of biomass, the production of hydrogen and bio-fuels such as gasoline and diesel.[47–50] The present work aims to develop a novel and environmentally friendly approach to efficiently producing the direct reduced iron (named the bio-oil-based DRI route) through a systematic experimental process development and process integration study on bio-oil reforming and iron ores reduction. In particular, the study of the bio-oil-based DRI route, with an emphasis on the bio-oil reforming process, would be helpful to promote real applications in producing high value-added products by using biomass (*e.g.*, biomass-derived H_2 and DRI). The green DRI process with a high reduction efficiency and real environmental benefits would, potentially, be a useful route to produce DRI from biomass.

2. Results and discussion

2.1 Bio-oil reforming process

2.1.1 Features of bio-oil reforming. In this work, the reducing gases (H_2-rich mixture gases) were first produced by the steam reforming of bio-oil, followed by the elimination of CO_2 *via* a purification process, and were then used for the direct reduction of iron oxides. The steam reforming of bio-oil over the $Ni–Cu–Zn–Al_2O_3$ catalyst (Ni : Cu : Zn : Al = 2 : 1 : 1 : 2) was carried out to investigate the features of the mixture gases from the bio-oil. The bio-oil used in this work was a pre-treated one (*i.e.*, obtained by distilling crude bio-oil derived from the pyrolysis of sawdust). The oxygenated organic compounds in the pre-treated bio-oil are represented by the chemical formula $CH_{2.03}O_{0.67}{\cdot}0.89H_2O$ (Table 5). The C, H, N, O, and S contents of the biomass, the crude bio-oil and the pre-treated bio-oil are shown in Table 5. The performance of the bio-oil reforming is mainly controlled by the reforming temperature ($T_{reforming}$) for a given catalyst.[46,51,52] To investigate the features of the mixture gases from bio-oil reforming, the bio-oil reforming was carried out under different temperatures, whilst other experimental conditions (*i.e.*, S/C (the ratio of steam to carbon fed) and GHSV (gas hourly space velocity) *etc.*) were kept constant. The reforming of bio-oil was tested at $T_{reforming}$ = 300–600 °C, S/C = 6.1, GHSV = 6300 h^{-1}, P = 1.1 atm. Fig. 1 shows the effects of the reforming temperature on the carbon conversion, the hydrogen yield, and the dry gas composition (*i.e.*, H_2, CO_2, CO, CH_4) over the $Ni–Cu–Zn–Al_2O_3$ catalyst. The reforming performance of the bio-oil was significantly enhanced by the reforming temperature in the catalytic bed. The carbon conversion was only about 17.6% at 300 °C and up to 96.8% at 600 °C. On increasing the temperature from 300 to 600 °C, the hydrogen yield increased remarkably, giving a maximum value of about 93.8% within our investigated region.

In addition, the present results show that hydrogen is major product (59.1–69.6 vol%) together with a smaller amount of by-products of CO_2 (15.6–29.6 vol%) and CO (0.8–21.6 vol%). A trace amount of CH_4 (<5 vol%) was also observed in the

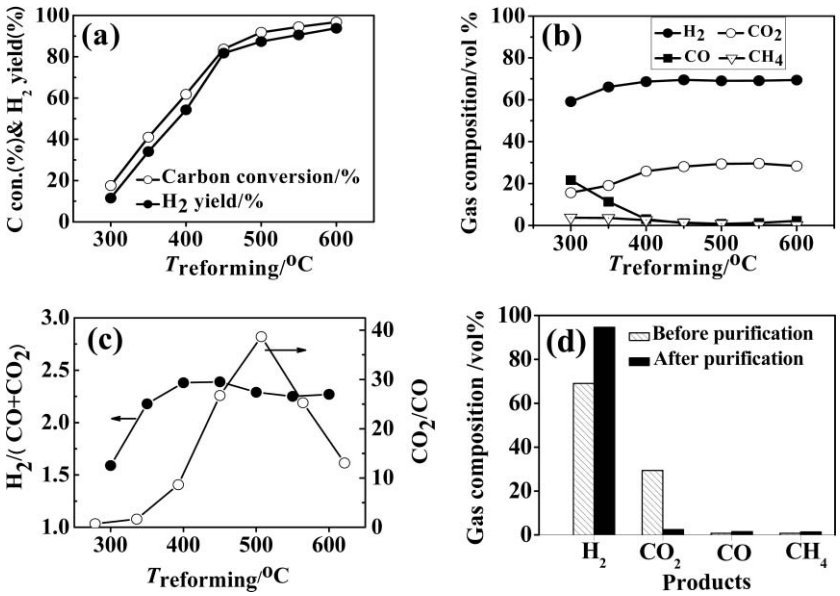

Fig. 1 Influence of the reforming temperature ($T_{reforming}$) on (a) the carbon conversion and the hydrogen yield, (b) dry gas compositions and (c) the volume ratios of $H_2/(CO + CO_2)$ and CO_2/CO from the steam reforming of bio-oil over the Ni–Cu–Zn–Al_2O_3 catalyst. (d) Typical reducing gas compositions before and after the purification. Reforming conditions: $T_{reforming} = 500$ °C, S/C = 6.1, GHSV = 6300 h^{-1}, and $P = 1.1$ atm.

effluent carbonaceous compounds in our investigated ranges. As shown in Fig. 1(b), the dry gas composition also depends on the reforming temperature. The concentration of CO decreased with increasing temperature, accompanied by an increase of the CO_2 content. The distribution of the unreformed by-products of CH_4 is near zero over 450 °C. As the temperature rises from 300 to 450 °C, the volume ratio of $H_2/(CO + CO_2)$ increases from 1.6 to 2.4 (Fig. 1(c)), and then gradually decreases over 450 °C. The CO_2/CO ratio reaches about 39 near 500 °C, which indicates that the mixture gas derived from the bio-oil reforming using the Ni–Cu–Zn–Al_2O_3 catalyst is a rich H_2/CO_2 one. The reforming reactions are generally endothermic and favored by high temperature, leading to a higher carbon conversion and H_2 yield at higher temperature. In contrast, the water–gas shift reaction is exothermic and favors lower temperatures. The distribution of products in the reforming processes of the bio-oil is mainly determined by the reforming reactions between various oxygenated organic compounds and water, secondary cracking of the compounds, the reforming reactions of the fragments as well as the water–gas shift reaction *etc.*, which is further investigated in the following sections. Moreover, the mixture gas from the bio-oil reforming generally contains 20–30 vol% CO_2. To increase the reduction efficiency of the iron ores, most of the CO_2 should be separated from the mixture gas. It is better that the content of CO_2 decreases to below 10 vol% in the mixture gas. To simplify the experimental process, the mixture gas from the reforming reactor was simply purified by removing CO_2 *via* a NaOH or Na_2CO_3 solution. After the CO_2 absorption (10% NaOH) and dry treatment, the content of hydrogen increased remarkably to about 94.6 vol% and the content of CO_2 decreased to below 3.0 vol% in the mixture gas (Fig. 1d).

Moreover, the Ni–Cu–Zn–Al_2O_3 catalyst may be one of most suitable candidates for the bio-oil reforming because this non-noble metal catalyst can efficiently reform the bio-oil to H_2 and CO_2 at a lower operating temperature (450–500 °C, Fig. 1), much lower than that using the conventional NiO-based catalysts (750–850 °C).[44–47] The carbon conversion of the bio-oil using the 18 wt% NiO/Al_2O_3 catalyst was very low (about 14.7%) at 400 °C, and even at 600 °C was only about 60%.[49] However, a hydrogen yield of 87.4% with a 91.8% carbon conversion in the bio-oil was obtained by using the Ni–Cu–Zn–Al_2O_3 catalyst at 500 °C. Lower operating temperatures using the Ni–Cu–Zn–Al_2O_3 catalyst in the bio-oil reforming would be due to higher activity for the bio-oil reforming reactions, the decomposition of the oxygenated organic compounds, and the water-gas shift reaction over this catalyst, as addressed in the next sections.

2.1.2 Bio-oil decomposition. The reaction pathways in the bio-oil steam reforming process are very complex and a lot of potential intermediates and products may be formed. The reaction network consists of a complex set of numerous reactions with multiple pathways depending on the bio-oil used and the catalyst selected and the operating conditions. At least three different types reactions should be considered: (1) the steam reforming of the oxygenated organic compounds ($C_nH_mO_k$) in the bio-oil ($C_nH_mO_k + (n-k)H_2O \rightarrow nCO + (n + m/2 - k)H_2$); (2) the decomposition of the oxygenated organic compounds ($C_nH_mO_k \rightarrow C_xH_yO_z$ + other fragments or gaseous small molecules); (3) the water–gas shift (WGS) reaction ($CO + H_2O \rightarrow CO_2 + H_2$). To further understand bio-oil reforming over the Ni–Cu–Zn–Al_2O_3 catalyst, studies on the bio-oil decomposition, the water–gas shift reaction, the catalyst inactivity, and the alteration of the catalyst properties after the reforming were also carried out. It should be pointed out that both the crude bio-oil and the pretreated one contained about 20–40 wt% H_2O (Table 5). To avoid the influence of water on the decomposition of the bio-oil, the pretreated bio-oil was further dehydrated by a multiple extractions method using *n*-butanol dehydrant (the weight ratio between bio-oil and dehydrant = 1 : 2). The water content in the resulting bio-oil after the extraction was less than

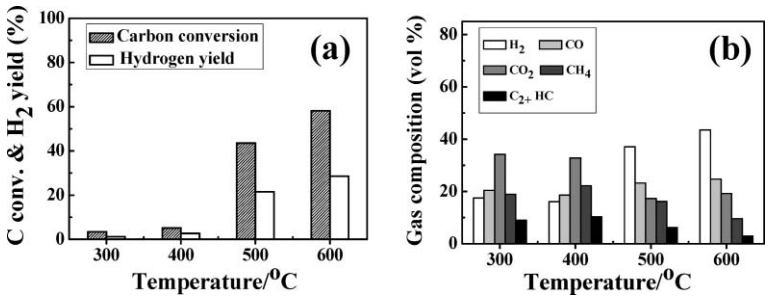

Fig. 2 Decomposition of the oxygenated organic compounds in the extracted bio-oil over the Ni–Cu–Zn–Al_2O_3 catalyst. The effect of temperature on (a) carbon conversion and hydrogen yield, and (b) the composition of the gaseous products from the decomposition of compounds, respectively. Conditions: $T_{decomposition}$ = 300–600 °C, GHSV = 5000 h^{-1}, and P = 1.1 atm.

2 wt%. As shown in Fig. 2, at temperatures lower than 400 °C, the carbon conversion from the bio-oil decomposition over the Ni–Cu–Zn–Al_2O_3 catalyst was very low (<5%). On increasing the temperature from 300 to 600 °C, the carbon conversion from the bio-oil decomposition increased remarkably from about 3 to 58% within our investigated region (Fig. 2(a)). The main gas products observed from the decomposition are H_2, CO, CO_2, H_2O, CH_4, and other hydrocarbons (C_2H_4, C_2H_6, C_2H_2, C_3H_6, and C_3H_8 *etc.*) (Fig. 2(b)). The selectivities of H_2 and CO slightly increased with increasing temperature, accompanied by a selectivity decrease for the hydrocarbons. The above results indicated that the Ni–Cu–Zn–Al_2O_3 catalyst efficiently dissociates the oxygenated organic compounds in the bio-oil over 500 °C.

2.1.3 Water–gas shift reaction. The water–gas shift (WGS) reaction ($CO + H_2O \rightarrow CO_2 + H_2$) is a very important side reaction that affects the equilibrium of both CO and CO_2 in the reforming of bio-oil. The WGS reaction is an encouraged elementary step for the reforming of bio-oil, because it can enhance the hydrogen yield. To investigate the WGS activity over the Ni–Cu–Zn–Al_2O_3 catalyst, the conversion of CO to CO_2 was tested using a model mixture of H_2O/CO/Ar (54 : 9 : 37 in vol% ratio, S/C = 6.0). As shown in Fig. 3, in the low temperature range (<300 °C), the conversion of CO increases with increasing temperature, reaching near complete conversion (about 100%) at 400 °C. Further increasing the temperature to over 500 °C will lead to a decrease in the CO conversion. In addition, CO is mainly converted into CO_2 with a selectivity of 87–100% through the WGS reaction ($CO + H_2O \rightarrow CO_2 + H_2$, ΔH_{298} = –41.1 kJ mol^{-1}), accompanied by the formation of a small amount of methane around 400 °C through the methanation reaction ($CO + 3H_2 \rightarrow CH_4 + H_2O$, ΔH_{298} = –205.9 kJ mol^{-1}). This suggests that the Ni–Cu–Zn–Al_2O_3 catalyst has a much higher WGS activity in the range of 300–600 °C.

2.1.4 Catalyst stability. The stability of the catalyst in bio-oil reforming was tested by measuring the carbon conversion, the yield of hydrogen and the changes in product composition as a function of the time on stream. As shown in Fig. 4, no obvious changes in the carbon conversion, the yield of hydrogen and the product distribution were observed for about the first 10 h under typical reforming conditions ($T_{reforming}$ = 500 °C, S/C = 6.9, GHSV = 6300 h^{-1}, and P = 1.1 atm). An obvious decrease in the catalytic activity was observed for a longer term test. For example, the hydrogen yield gradually decreases by about 10% (from about 90 to 80%) after about 20 h reforming, and dropped to 50% of the initial value after about 40 h. In addition, the deactivated catalyst can be partly regenerated through oxidation treatment *via* the ambient oxygen (not shown here). It was also noticed that the lifetime of the Ni–Cu–Zn–Al_2O_3 catalyst in bio-oil reforming (Fig. 4) is much longer than that of the NiO-based catalyst.[39,45] The catalyst inactivity observed in the bio-oil reforming process could be mainly attributed to C deposition and partly to the alteration of the catalyst properties as described below.

2.1.5 Changes of catalyst properties in bio-oil reforming. To further clarify the catalyst deactivation, we investigated the amount of the carbon deposition, both on the catalyst surface and in the catalyst body, the sulfur deposition and the characteristic alterations of the catalyst after the reforming *via* ICP-AES

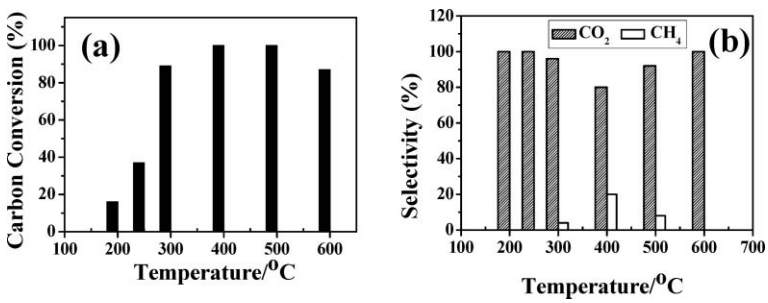

Fig. 3 WGS activity over the Ni–Cu–Zn–Al_2O_3 catalyst. (a) CO conversion, and (b) the selectivities toward CO_2 and CH_4. Reaction conditions: CO : Ar = 1 : 4 (in vol% ratio), f(CO + Ar) = 100 ml min^{-1}, $f(H_2O)$ = 0.1 ml min^{-1}, $T_{reforming}$ = 200–600 °C, S/C = 6.0, GHSV = 5000 h^{-1}, and P = 1.1 atm.

Table 1 Chemical and physical properties of fresh and used Ni–Cu–Zn–Al_2O_3 catalysts

Samples[a]	S_{BET} [b]/m^2 g^{-1}	PV [b]/cm^3 g^{-1}	d_{xrd} [c]/nm	$[C]_{surface}$ [d](wt%)	$[C]_{body}$ [e](wt%)	$[S]_{surface}$ [d](wt%)	$[S]_{body}$ [e](wt%)
No. 1	210.0	0.50	11.4	0.2	0.2	not detectable	0.007
No. 2	85.0	0.42	46.0	10.9	8.7	not detectable	0.005

[a] No. 1: the fresh Ni–Cu–Zn–Al_2O_3 catalyst; No. 2: the used Ni–Cu–Zn–Al_2O_3 catalyst after bio-oil reforming for 50 h (reforming conditions: $T_{reforming}$ = 500 °C, S/C = 6.9, GHSV = 6300 h^{-1}, and P = 1.1 atm). [b] Surface area (S_{BET}) and pore volume (PV) evaluated from N_2 adsorption–desorption isotherms. [c] Average granule size estimated from the peaks of XRD by the Scherrer equation. [d] The elemental contents of C and S on the catalyst surface were measured by XPS analysis. [e] The elemental contents of C and S in the catalyst body were measured by ICP-AES and TGA analyses.

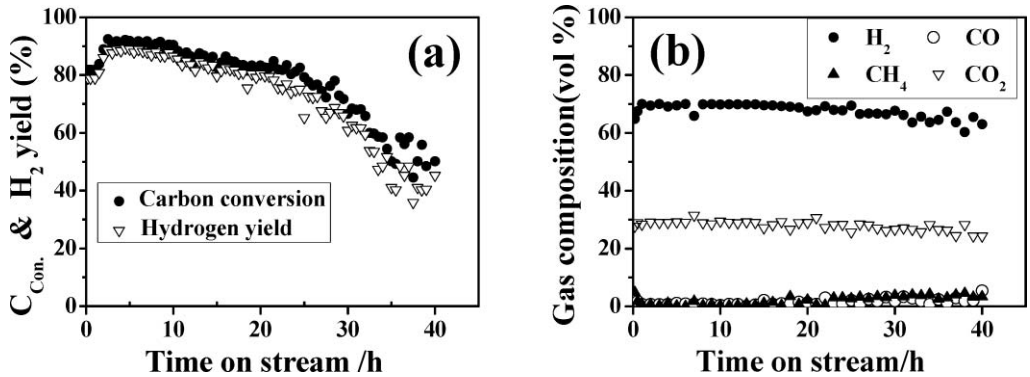

Fig. 4 Stability curves measured under typical bio-oil reforming of over the Ni–Cu–Zn–Al_2O_3 catalyst. (a) Carbon conversion and hydrogen yield, (b) the gaseous product distribution. Reforming conditions: $T_{reforming}$ = 500 °C, S/C = 6.9, GHSV = 6300 h^{-1}, and P = 1.1 atm.

(inductively coupled plasma-atomic emission spectroscopy), TGA (thermogravimetric analysis), XPS (X-ray photoelectron spectroscopy), XRD (X-ray diffraction), and N_2 adsorption–desorption isotherms analyses. The results are summarized in Table 1. The amounts of carbon deposited on the catalyst surface and in the catalyst body were about 10.9 wt% and 8.7 wt%, respectively, for 50 h reforming. The amounts of sulfur deposited on the catalyst surface were not detectable within the detection limitation for the same reforming duration. In comparison with the fresh catalyst, the BET surface areas of the used ones also decreased, accompanied by an increase in the size of the particles. Generally, C or S deposition will block the active cites, leading to a decrease in the catalyst activity.[42–49] The decrease of the BET surface area or the increase of the particle size may also reduce the catalyst activity.[42,49] Accordingly, the catalyst inactivity observed in the bio-oil reforming process could be partly attributed to C deposition and partly to alteration of the catalyst properties.

Furthermore, alterations to the structural and atomic states after the reforming of bio-oil were investigated in detail by XRD and XPS analyses. Fig. 5 shows typical XRD spectra for (A) the pristine Ni–Cu–Zn–Al_2O_3 catalyst, and (B) the used ones after the reforming of bio-oil for 50 h. For the fresh catalyst (Fig. 5(A)), the oxide states were observed. However, the XRD pattern for the used catalyst after reforming is quite different from that of the fresh one. As shown in Fig. 5(B), a series of new peaks appeared for the used catalysts, after reforming, corresponding to the metallic phases (*i.e.*, Ni^0, Cu^0, and Zn^0). This means that the oxide states were reduced to the metallic states during the bio-oil reforming process. The reduction of the oxide states is mainly attributed to the reduction by hydrogen formed in the reforming of bio-oil (*i.e.*, $M^{2+} + H_2 \rightarrow M^0$). Alterations in the atomic states of the catalyst's surfaces before

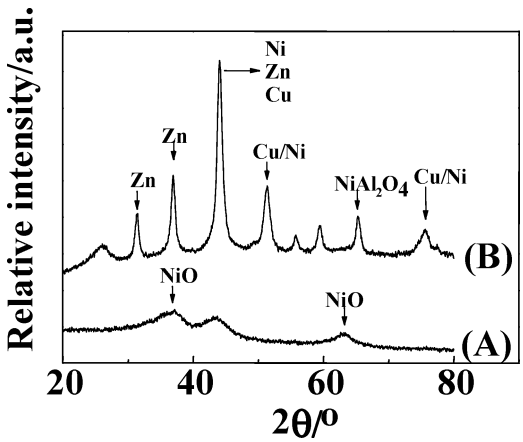

Fig. 5 XRD spectra for (A) fresh Ni–Cu–Zn–Al_2O_3 catalyst, (B) the used catalyst after steam reforming of bio-oil for 50 h. Reforming conditions: $T_{reforming}$ = 500 °C, S/C = 6.1, GHSV = 6300 h^{-1}, and P = 1.1 atm.

and after the reforming of bio-oil were also investigated by XPS measurements. As shown in Fig. 6, binding energies of about 855.5 and 861.7 eV were observed for the pristine catalyst, which were assigned to the main line of $Ni^{2+}(2p_{3/2})$ and its satellite, respectively. After the catalytic reforming of bio-oil, a new peak was observed near 852.6 eV in the Ni XPS spectrum (Fig. 6), corresponding to the peak of the metallic $Ni^0(2p_{3/2})$. The main line and satellite of $Ni^{2+}(2p_{3/2})$ disappeared synchronously. The above results clearly show that Ni was in the +2 "formal" oxidation state in the fresh catalyst prepared and almost all of the Ni^{2+} (*i.e.*, the NiO phase) was reduced to metallic Ni^0 after the catalytic reforming of bio-oil for 50 h. Fig. 6 also displays the Cu XPS spectra (930–970 eV) and the Zn XPS spectra (1020–1028 eV) from the three samples mentioned above.

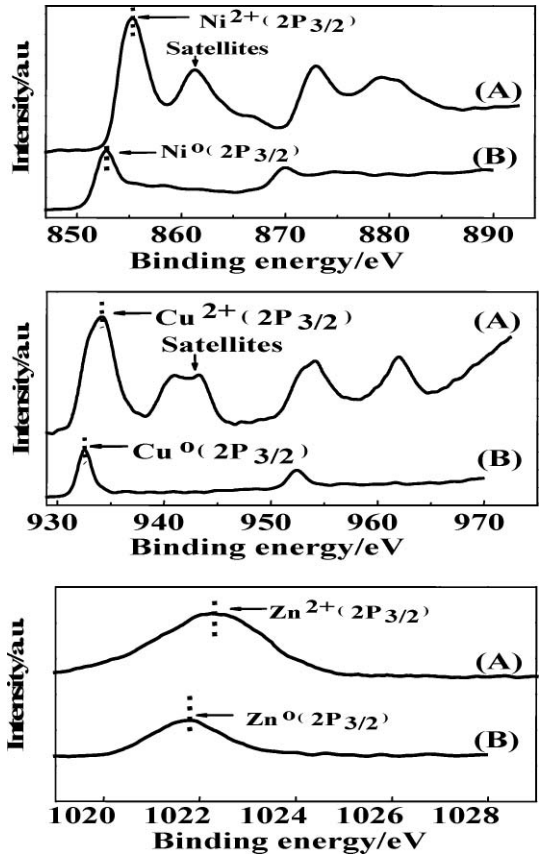

Fig. 6 Ni/Cu/Zn XPS spectra (from top to bottom panels) for (A) fresh Ni–Cu–Zn–Al_2O_3 catalyst, (B) the used catalyst after steam reforming of bio-oil for 50 h. Reforming conditions: $T_{reforming}$ = 500 °C, S/C = 6.1, GHSV = 6300 h^{-1}, and P = 1.1 atm.

The reductions from +2 "formal" oxidation states of $Cu^{2+}(2p_{3/2})$ (933.4 eV) and $Zn^{2+}(2p_{3/2})$ (1022.3 eV) to the metallic $Cu^0(2p_{3/2})$ (932.5 eV) and $Zn^0(2p_{3/2})$ (1021.8 eV) states were also identified after the reforming of bio-oil.

2.2 Production of DRI by bio-oil-based reducing gases

One of main aims in this work is to efficiently produce DRI (direct reduced iron) using bio-oil and ores with two serial flowing fixed bed reactors (*i.e.*, the reforming reactor and the reduction reactor), where the steam reforming of bio-oil is performed in the reforming reactor and the reduction of the oxidation iron is carried out in the reduction reactor. This design has some advantages such as easy controlling for different reaction parameters and efficiently avoiding the pollutants from the unreformed bio-oil and coke-deposition during bio-oil reforming. Three powder samples (hematite, limonite and magnetite) with the average size of 0.1–0.2 mm and hematite pellets with an average size of 8–12mm were used for the reduction tests. The main compositions of these ores are listed in Table 6 in the Experimental section. The reduction conditions were set up with the reduction temperature = 650–850 °C, the flowing speed of the reducing gases = 100 ml min^{-1}, the reduction duration = 1 h, and the fed amount of the iron ores was 20 g. The bio-oil-based reducing gas (H_2 : CO: CO_2 : CH_4 = 94.6 : 1.6 : 2.5 : 1.3) was produced on-line by the reforming of bio-oil under a preferable reforming condition (the reforming temperature = 500 °C, S/C = 6.1, GHSV in the reforming reactor = 6300 h^{-1}, pressure = 1.1 atm). Table 2 shows the performance of the DRI including total iron content (TFe in wt%), metallic iron content (MFe in wt%) and the metallization (the ratio of MFe to TFe in the DRI product) at different reduction temperatures. When the reduction temperature was 650 °C, the content of the metallic iron (MFe (wt%)) in the resulting DRI was very low, being about 12.1, 11.8 and 19.9 wt% for the limonite, magnetite and hematite ore powders. On increasing the reduction temperature from 650 to 850 °C, the content of the metallic iron increased considerably to 63.4, 67.6 and 67.2 wt% for the above ore powders. On the other hand, the metallization in the ore reduction process, defined as the ratio of metallic iron content of DRI to total iron content of DRI, increased remarkably from 21.3 to 94.7% for the magnetite on increasing the reduction temperature from 650 to 850 °C. High metallization for production of DRI from three ore powders (limonite, hematite and magnetite), as well as the pellet sample, ranging from 93 to 97%, was obtained at 850 °C for 1 h reduction.

Table 2 The performance of the bio-oil-based DRI derived from the hematite, limonite and magnetite powders and hematite pellets at different reduction temperatures. Reduction time = 1 h; pressure = 1.1 atm. The data given in this table are the averaged values from the three tests

Samples	T/°C	TFe (wt%)	MFe (wt%)	Metallization (%)
Limonite powder	650	52.7	12.1	23.0
Limonite powder	750	57.0	38.0	66.7
Limonite powder	850	68.1	63.4	93.1
Magnetite powder	650	55.2	11.8	21.3
Magnetite powder	750	58.4	29.6	50.7
Magnetite powder	850	71.4	67.6	94.7
Hematite powder	650	56.0	19.9	35.5
Hematite powder	750	61.5	47.8	77.8
Hematite powder	850	70.1	67.2	95.9
Hematite pellet	750	80.6	49.4	61.3
Hematite pellet	850	90.0	86.6	96.2

XRD analyses have been carried out to further investigate the various oxide and metallic phases in the DRI products. Fig. 7 shows typical XRD spectra from (A) the limonite raw material (L-raw), (B) the DRI sample reduced at 650 °C for 1 h (L-DRI(650 °C, 1h)), and (C) the DRI sample reduced at 850 °C for 1 h (L-DRI(850 °C, 1h)). The bio-oil reforming conditions were: T = 500 °C, S/C = 6.1, GHSV = 6300 h^{-1}, P = 1.1 atm. The reduction conditions were: T = 650–850 °C, reducing gases composition: H_2 (94.6 vol%), CO (1.6 vol%), CO_2 (2.5 vol%), CH_4 (1.3 vol%), flowing speed = 100 ml min^{-1}, reduction time = 1 h and the averaged samples size = 0.1–0.2 mm. For the limonite raw material, the goethite (FeO(OH)) phase at 2θ = 21.1, 36.6 and 33.2° was observed. For the DRI sample reduced at 650 °C, new XRD peaks appeared at 2θ = 44.6, 82.3 and 65.0° respectively, corresponding to the diffraction crystal phase of Fe. This means that part of FeO(OH) was reduced to the metallic Fe at the reduction temperature of 650 °C. In particular, it was also observed that the intermediate diffraction phases of Fe_3O_4 (2θ = 35.4, 62.5 and 56.9°) and FeO (2θ = 41.7, 36.3 and 61.9°) were formed. Apart from a trace of intermediate phase FeO, almost all of the oxidation iron phase (FeO(OH)) was completely converted into the metallic Fe for the DRI sample reduced at 850 °C for

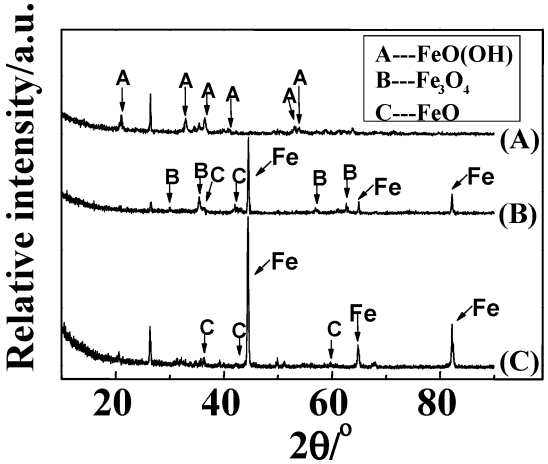

Fig. 7 Typical XRD patterns from (A) the limonite raw material, (B) the DRI sample reduced at 650 °C for 1 h, (C) the DRI sample reduced at 850 °C for 1 h.

1 h, which also agreed with the results from the metallization analysis (Table 2). According to the XRD analysis, the reduction of limonite (goethite) seems to occur through a stepwise process, *i.e.*, FeO(OH) → Fe_3O_4 → FeO → Fe. The observed phases are listed in Table 3. Moreover, the mean particle sizes of Fe were also estimated by analyzing the strongest diffraction peak of Fe at $2\theta = 44.6321°$. The mean particle sizes were calculated by the Scherrer equation:[53]

$$d = \frac{K\lambda}{\beta\cos\theta} \quad (1)$$

where λ is the wavelength of the X-ray source ($\lambda_{Cu\,K\alpha}$ = 0.154056 nm), K is the Scherrer constant, β is the full-width at half maximum (FWHM), and θ is the diffraction angle of the X-ray diffraction. As can be seen in Table 3, the mean diameter of the particles increased from 31.75 to 84.57 nm when the reduction temperature increased from 650 to 850 °C. The increase in the size of crystallites at higher reduction temperatures may reflect the congregation of the particles.

Fig. 8 shows typical XRD spectra from (A) the magnetite raw material (M-raw), (B) the DRI sample reduced at 650 °C for 1 h (M-DRI(650 °C, 1h)) and (C) the DRI sample reduced at 850 °C for 1 h (M-DRI(850 °C, 1h)). For the magnetite raw material, the main composition of the Fe_3O_4 phase at 2θ = 35.4, 62.5 and 56.9° was observed. Besides the diffraction peaks of Fe, the X-ray diffraction peaks of FeO at $2\theta = 41.7$, 36.3 and 61.9° were clearly observed for the DRI sample reduced at 650 °C. For the DRI sample reduced at 850 °C for 1 h, strong diffraction peaks of Fe, together with a trace amount of FeO at 2θ = 41.7, 36.3 and 61.9°, were observed. The oxidized iron phase of Fe_3O_4 was not found for the DRI sample reduced at 850 °C for 1 h, indicating that the oxidation iron phase of Fe_3O_4 was nearly completely converted into the metallic Fe or FeO. Based on the above the XRD results, the reduction of Fe_3O_4 may carry through a stepwise process *via* Fe_3O_4 → FeO → Fe.

Fig. 9 shows the XRD spectra from (A) the hematite raw powder material (H-raw), (B) the DRI sample reduced at 650 °C for 1 h (H-DRI(650 °C, 1h)) and (C) the DRI sample reduced at 850 °C for 1 h (H-DRI(850 °C, 1h)), respectively. For the

Table 3 Properties of the raw ores and the corresponding bio-oil-based DRI products

Sample	Observed phase from XRD			d_{Fe}/nm[a]
L-Raw	FeO(OH)[b]			
L-DRI (650 °C, 1h)	Fe_3O_4[c]	FeO[d]	Fe[e]	31.75
L-DRI (850 °C, 1h)	FeO		Fe	84.57
M-Raw	Fe_3O_4	Fe_2O_3[f]		
M-DRI (650 °C, 1h)	Fe_3O_4	FeO	Fe	34.69
M-DRI (850 °C, 1h)	FeO		Fe	50.83
H-Raw	Fe_2O_3	Fe_3O_4		
H-DRI (650 °C, 1h)	Fe_3O_4	FeO	Fe	35.56
H-DRI (850 °C, 1h)			Fe	45.66

[a] Average Fe crystalline size estimated from the peak of XRD by the Scherrer equation. [b] ref. PDF-29-0713 card (International Centre for Diffraction Data (ICDD), 2002). [c] ref. PDF-19-0629 card (International Centre for Diffraction Data (ICDD), 2002). [d] ref. PDF-06-0615 card (International Centre for Diffraction Data (ICDD), 2002). [e] ref. PDF-06-0696 card (International Centre for Diffraction Data (ICDD), 2002). [f] ref. PDF-33-0664 card (International Centre for Diffraction Data (ICDD), 2002).

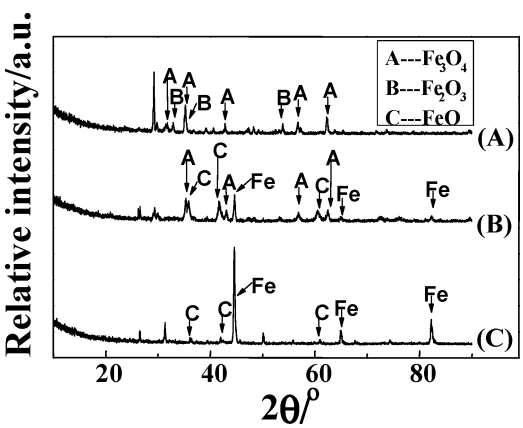

Fig. 8 Typical XRD patterns from (A) the magnetite raw material; (B) the DRI sample reduced at 650 °C for 1 h, (C) the DRI sample reduced at 850 °C for 1 h.

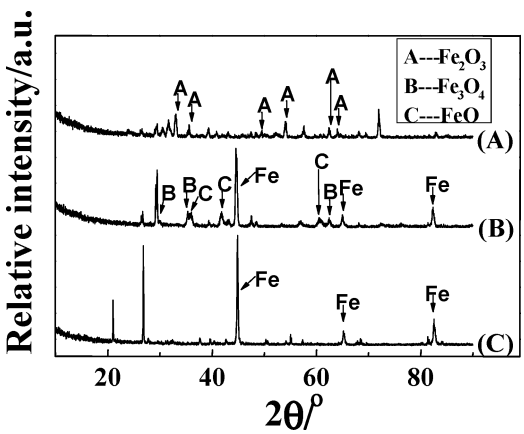

Fig. 9 Typical XRD patterns from (A) the hematite powder material, (B) the DRI sample reduced at 650 °C for 1 h, (C) the DRI sample reduced at 850 °C for 1 h.

Table 4 Comparison of DRI produced by the natural gas-based, coal-based and bio-oil-based processes

DRI processes	Natural gas-based DRI (Midrex, HYL *etc.*)[a]	Coal-based DRI (SL, RN, DRC *etc.*)[b]	Bio-oil-based DRI (present work)
Raw materials	Natural gas and iron ores	Coal and iron ores	Bio-oil from biomass and iron ores
Process description	DRI produced from direct reduction of iron ores *via* the reducing gases from the reforming of natural gas	DRI produced from direct reduction of iron ores *via* the mixture of iron ores, additive and coal at high temperature	DRI produced from direct reduction of iron ores *via* the reducing gases from the stream reforming of bio-oil from biomass
Main operating conditions	Reforming temperature = 800–850 °C, Reduction temperature: = 700–1000 °C	Reduction temperature = 800–1300 °C.	Reforming temperature 450-550 °C, Reduction temperature:700-850 °C.
Material consumed per ton DRI	10.0–18.9 (GJ natural gas)	14.8–19.3 (GJ coal)	0.5–0.7 (ton bio-oil)
Cost of DRI (US$/(ton DRI))	71–252	123–254	210–310[c]
Optimum location	Natural gas-rich area	Coal-rich area	Globally available
Real CO_2 emissions	50–70 kg CO_2/(GJ natural gas) or (500–1330 kg CO_2/(ton DRI))	90–110 kg CO_2/(GJ coal) or (1300–2100 kg CO_2/(ton DRI))	(450–770 kg CO_2/(ton DRI))[d]
Net CO_2 emissions	500–1330 kg CO_2/(ton DRI)	1300–2100 kg CO_2/(ton DRI)	None (CO_2 circulation in atmosphere)

[a] Ref. 3, 11, 12 and 26. [b] Ref. 3, 11, 12 and 26. [c] The cost of DRI produced by present bio-oil-based process was estimated by the total cost as listed below. 1) The cost of the bio-oil derived from biomass (about 800–1000 RMB/(ton bio-oil) in China, or about 117–146 US$/(ton bio-oil)); 2) the cost of the iron ores (450–700RMB/(ton ore) in China, or about 66–102 US$/(ton ore)); 3) the cost of water (3 RMB/(ton water) in China, or about 0.5 US$/(ton water)); 4) the cost of the catalyst (100–150 RMB/(kg catalyst) in China, or about 15–22 US$/(kg catalyst)); 5) the energy consumption in the pre-treating process of the bio-oil, the production of the reducing gas from the bio-oil reforming, and production of DRI from the iron ores, based on the combustion of the bio-oil (0.2–0.4 ton bio-oil/(ton DRI) with the heat value of 16–18 MJ kg^{-1}); 6) the cost of CSS (CO_2 separating and saving) based on the PSA processing (pressure swing adsorption, about 300 RMB/(ton CO_2) in China, or about 43 US$/(ton CO_2)). [d] Real CO_2 emission mainly includes two parts, *i.e.*, the amount of CO_2 emitted in the production process of the reducing gas derived from bio-oil reforming (about 132 kg CO_2/(ton DRI)), and that for providing energy through the combustion of the bio-oil (about 318–638 kg CO_2/(ton DRI)).

hematite raw material, the XRD results show that the ore is mainly composed of Fe_2O_3 together with Fe_3O_4. The intermediate diffraction peaks of the FeO phase were also observed for the DRI sample from hematite ore. Almost complete reduction of the oxidized irons was also obtained at 850 °C for 1 h by using the bio-oil-based reducing gases. Congregation of the particles was also observed for the magnetite and hematite, leading to an increase in the size of the crystallites at higher reduction temperatures (Table 3).

It was noticed that the reducing species from the steam reforming of bio-oil mainly contained H_2 together with small amount of CO_2, CO and CH_4, and the content of CH_4 was low (<2 vol%) in the effluent gaseous compounds from the reforming reactor. Thus, it is considered that the oxidized iron is essentially reduced by H_2 accompanied by CO. Reduction of hematite by hydrogen would proceed in complex steps *via* magnetite (Fe_3O_4) and the wüstite intermediates (FeO) according to previous work,[22,54] which can be represented by the following paths:

$$3Fe_2O_3 + H_2 \rightarrow 2Fe_3O_4 + H_2O \quad (2)$$

$$Fe_3O_4 + 4H_2 \rightarrow 3Fe + 4H_2O \quad (3)$$

$$(1 - x)Fe_3O_4 + (1 - 4x)H_2 \rightarrow 3Fe_{1-x}O + (1 - 4x)H_2O \quad (4)$$

$$Fe_{1-x}O + H_2 \rightarrow (1 - x)Fe + H_2O \quad (5)$$

Generally, the wüstite intermediate is unstable under thermodynamic equilibrium. According to present XRD results, both the magnetite (Fe_3O_4) and wüstite (FeO) were observed during the reduction process of Fe_2O_3 (Fig. 7–9). Accordingly, the reduction of oxidized iron for present raw ores *via* the bio-oil-based reducing gases would proceed through the following paths:

$$\text{magnetite: } Fe_3O_4 \rightarrow FeO \rightarrow Fe \quad (6)$$

$$\text{limonite: } Fe_{+3}O(OH) \rightarrow Fe_3O_4 \rightarrow FeO \rightarrow Fe \quad (7)$$

$$\text{hematite: } Fe_2O_3 \rightarrow Fe_3O_4 \rightarrow FeO \rightarrow Fe \quad (8)$$

On the other hand, CO can also reduce the iron-oxide phases into metallic iron during the course of reduction *via* three sequential stages of iron oxide reduction as follows:

$$\text{hematite to magnetite: } 3Fe_2O_3 + CO \rightarrow 2Fe_3O_4 + CO_2 \quad (9)$$

$$\text{magnetite to wüstite: } Fe_3O_4 + CO \rightarrow 3FeO + CO_2 \quad (10)$$

$$\text{wüstite to iron: } FeO + CO \rightarrow Fe + CO_2 \quad (11)$$

It is noted that the content of CO (1–4 vol%) is much lower than that of H_2 in the effluent gaseous compounds from the reforming reactor. Thus, the present DRI process should be mainly attributed to the reduction of oxidized iron with hydrogen.

Finally, Table 4 shows a comparison and evaluation for three different DRI processes based on the raw material used for producing reducing agents (*i.e.*, the natural gas-based, coal-based and bio-oil-based DRI processes). Currently, two main routes, the natural gas-based (with a present market share of

75%) and coal-based DRI processes, have been well developed and commercialized for production of direct reduced iron (DRI).[4,7,9,10] The operating temperature in the present bio-oil-based DRI process seems lower than those in the natural gas-based and coal-based DRI processes. The net emission amount of CO_2 was considered to be near zero because biomass has been proposed as a feedstock to produce hydrogen without a net increase in atmospheric CO_2.[16,36,55] The real amount of CO_2 produced in the bio-oil-based DRI process was about 450–770 kg CO_2/(ton DRI) (*i.e.*, the sum of about 132 kg CO_2/(ton DRI) in the bio-oil reforming together with about 318–638 kg CO_2/(ton DRI) for providing energy through the combustion of the bio-oil), which is obviously lower than those in the natural gas-based or coal-based DRI processes. Currently, the industrial CO_2 separating and saving (CCS) is realized by four major processes: (1) pressure-swing adsorption (PSA) (2) dissolvent absorption method, (3) membrane separation (MS) method and (4) low temperature processing.[56–58] The PSA and MS routes seem more attractive and commercially established for large-scale production of DRI (direct reduction iron) because these environmentally friendly processes may be suitable for separating CO_2 from the bio-oil-derived rich-H_2 mixture gas with a lower cost. In the present work, we mainly concentrated on the bio-oil-based DRI route with an emphasis on the bio-oil reforming and the performance of direct reduction of iron oxides. To simplify the experimental process, the mixture gas from the reforming reactor was simply purified by removing CO_2 *via* a NaOH or Na_2CO_3 solution. In addition, PSA processing was adopted in our scale-up research in a bench scale (2–5 kg DRI/h). Moreover, when we estimated the production cost of DRI using biomass (Table 4), the following items were mainly considered: (1) the cost of the raw materials including the biomass, the iron ores, the catalyst, the CO_2 absorbent as well as water used; (2) the cost of the energy consumption in the biomass pyrolysis, the bio-oil reforming, the pre-treatment of the crude bio-oil, and the iron ores reduction processes. The cost of the CO_2 separation and saving process was in reference to the data of 300 RMB/(ton CO_2) (or about 43 US$/(ton CO_2) derived from the industrial PSA technology.[59,60] From the viewpoint of economics, producing DRI from the bio-oil-based route seems to be somewhat more expensive in comparison with those of the natural gas-based and coal-based direct reduction processes. However, in view of growing environmental concerns and the depletion of fossil sources, the green DRI process using renewable biomass with a high reduction efficiency, relatively temperate operating conditions, contiguous competitive cost with natural gas-based or coal-based DRI and real environmental benefits, potentially, may be a useful route to produce DRI in future. In addition, production of DRI using renewable biomass was scaled-up from a bench scale (2–5 kg DRI/h), which includes four major sequential processes: (1) biomass pyrolysis, (2) bio-oil reforming, (3) CO_2 separation and (4) reduction of iron ores. This work is in progress.

3. Conclusion

(i) Bio-oil-based DRI route

A novel and environmentally friendly approach to efficiently produce direct reduced iron (the bio-oil-based DRI) was developed through a systematic experimental process development and process integration study on bio-oil reforming and iron ores reduction. The green DRI process with a high reduction efficiency, relatively temperate operating conditions, contiguous competitive cost with natural gas-based or coal-based DRI and real environmental benefits, potentially, may be a useful route to produce DRI from bio-oil or biomass in future.

(ii) Reforming catalyst and reforming process

The Ni–Cu–Zn–Al_2O_3 catalyst is one of most suitable candidates for bio-oil reforming because this non-noble metal catalyst can efficiently reform the bio-oil to H_2 and CO_2 at a lower operating temperature (450–500 °C), being much lower than that using the conventional NiO-based catalysts (750–850 °C).[44–47] The hydrogen yield of 87.37% with a 91.82% carbon conversion in the bio-oil was obtained by using the Ni–Cu–Zn–Al_2O_3 catalyst at 500 °C and S/C = 6.1. In addition, the lifetime of the Ni–Cu–Zn–Al_2O_3 catalyst in bio-oil reforming is also much longer than that of the NiO-based catalyst. Moreover, the features of the bio-oil reforming, the decomposition of oxygenated organic compounds, and the water–gas shift reaction over the Ni–Cu–Zn–Al_2O_3 catalyst have been investigated to further understand the bio-oil reforming process.

(iii) Bio-oil-based DRI process

Direct reduction of iron oxides for high efficient production of DRI was obtained by using real bio-oil-based rich-hydrogen reducing gases for different iron ores. The metallization for production of DRI from three ore powders (limonite, hematite and magnetite) and hematite pellets ranges from 93 to 97% at 850 °C for 1 h reduction. The main reduction steps for hematite and limonite were Fe_2O_3 (FeO(OH) for limonite) → Fe_3O_4 → FeO → Fe, and the reduction of magnetite would proceed though Fe_3O_4 → FeO → Fe. A comparison and evaluation for three different DRI processes (*i.e.*, the natural gas-based, coal-based and bio-oil-based DRI processes) was also made (Table 4). For separating and saving CO_2, the pressure-swing adsorption (PSA) or membrane separation (MS) technologies seem more suitable and commercially established for large-scale production of DRI due to the environmental benefits with a lower cost.

4. Experimental

Bio-oil

Bio-oil was produced by the fast pyrolysis of biomass in a circulating fluidized bed with a capacity of 120 kg h^{-1} of oil at our Lab (CN Pat., 01263584.7). The pyrolysis of biomass to produce bio-oil generally ran from 520 to 540 °C (heating rate = ~10^4 °C s^{-1}, residence time = < 2 s), followed by a fast cooling process. The main products of the fast pyrolysis of biomass consisted of liquid bio-oil (55–70 wt %), a mixture gaseous products, and charcoal. The bio-oil was comprised of different molecular weight products, derived from depolymerization and fragmentation reactions of three key biomass building blocks: cellulose, hemicellulose, and lignin. Hence, the elemental composition of bio-oil varied with different biomass feedstocks. Some physical and chemical properties of the typical

Table 5 Characteristics of pine wood sawdust, the crude bio-oil derived from the sawdust and pre-treated bio-oil used in this work

Characteristics	Wood sawdust[a]	Crude bio-oil	Pre-treated bio-oil
C (wt%)	46.21	54.50	48.5
H (wt%)	5.84	6.70	8.20
N (wt%)	0.52	0.30	0.10
O (wt%)[b]	47.43	38.48	43.20
S (wt%)	0.006	0.02	0.004
H_2O (wt%)	Dry-basis	21.0	39.3
Ash (wt%)	0.84	0.07	<0.01
Density (g cm^{-3})	0.28	1.28	1.13
LHV (MJ kg^{-1})	17.02	18.20	—
Chemical formula	$CH_{1.53}O_{0.78}$	$CH_{1.48}O_{0.53}{\cdot}0.32H_2O$	$CH_{2.03}O_{0.67}{\cdot}0.89H_2O$

[a] Dry-basis biomass. [b] By difference.

bio-oils derived from sawdust, rice husk, and cotton stalk powder were summarized in Table 5. The bio-oils contain a large number of complex compounds such as hydroxyaldehydes, hydroxyketones, sugars, carboxylic acids, phenolics, and so forth. These compounds are generally described by a chemical formula of $C_nH_mO_k{\cdot}xH_2O$. The crude biomass pyrolysis oil contain some amount of nonvolatile materials (35–40wt.%), such as sugars and oligomeric phenolics *etc*., which are generally difficult to be reformed and easily form carbon depositions on the catalyst surface leading to the fast deactivation of catalysts. Therefore, in this work, the crude bio-oil derived from sawdust was pretreated by vaporizing from 80 to 180 °C, and the volatile organic components of the crude bio-oil were then used for the reforming experiments. The amount of volatile organic components was about 50–60 wt % of the crude oil. Table 5 shows some chemical properties of crude bio-oil and the pretreated bio-oil derived from sawdust. The S and N contents in the biomass, in the crude bio-oil and the pre-treated one are also given in Table 5.

Material of iron ores

The iron ores used in this study were kindly supplied by the Maanshan Iron & Steel Co., Ltd. (Anhui Province, China). Table 6 shows main compositions of the iron ores of limonite, hematite and magnetite powders and hematite pellets, which were measured by X-ray fluorescence analysis (X-ray fluorescence analysis was performed on SHIMADZU XRF-1800 with Rh radiation). It was further confirmed by X-ray diffraction (XRD, on an X'pert Pro Philips diffractrometer with Cu Kα radiation.) that α-Fe_2O_3 and Fe_3O_4 dominate in the hematite and magnetite ore powders.

Reforming catalyst

The Ni–Cu–Zn–Al_2O_3 reforming catalysts with settled Ni : Cu : Zn : Al ratio near 2 : 1 : 1 : 2, which was based on the screening tests of the catalyst, were prepared by the co-precipitation method at a constant pH (9.0 ± 0.3) using respective metal nitrates as precursors and a mixed solution of NaOH (1M) and Na_2CO_3 (1M) as precipitants. The precipitate was dried overnight in an oven at 110 °C, then heated at 10 °C min^{-1} in air to 450 °C and calcined at 450 °C for 5 h to obtain the corresponding mixed oxide catalysts. The metallic element contents of the prepared catalysts (Ni: 23.96 wt%, Cu: 13.45 wt%, Zn: 13.12 wt%, Al: 9.36 wt%) were measured by inductively coupled plasma and atomic emission spectroscopy (ICP-AES, Atom scan Advantage of Thermo Jarrell Ash Corporation, USA). The Brunauer–Emmett–Teller (BET) surface area and the pore volume were about 210 m^2 g^{-1} and 0.5 cm^3 g^{-1}, respectively, which was evaluated from the N_2 adsorption–desorption isotherms obtained at 77 K over the whole range of relative pressures by using a COULTER SA 3100 analyzer.

Table 6 Main compositions (wt %) in the iron ores by X-ray fluorescence analysis

Ore	TFe	Al_2O_3	MgO	SiO_2	CaO	MnO
Limonite powder	51.76	3.91	0.08	12.34	0.35	0.54
Magnetite powder	54.69	0.21	0.34	5.40	8.78	0.03
Hematite powder	53.69	0.14	0.44	3.90	11.05	0.05
Hematite pellet	65.23	0.76	0.12	1.72	2.53	0.93

Reaction system

To obtain the direct reduced iron (DRI), the reducing gases were continuously produced by the steam reforming of the bio-oil, followed by the reduction process of the oxidation iron in the ores *via* the purified reducing gases. All experiments were performed in an atmospheric pressure. Fig. 10 (left) schematically shows the three main units in the present DRI production system, *i.e.*, the steam reforming of the bio-oil (Part 1), the unit for purification of the reducing gases and sampling (Part 2), and the unit for the reducing the oxidized iron (Part 3).

The steam reforming of the bio-oil was carried out in a continuous flow system (Part 1), using a quartz fixed-bed reactor (named the reforming reactor) under atmospheric pressure. The bio-oil was fed into the reactors using micro-injection pumps (Model: TS2-60, Longer Precision Pump). And the steam from the steam-generator was simultaneously fed into the reactors for adjusting the S/C ratio (mol. ratio of steam to carbon in the bio-oil fed). The above steam feed and the effluent gases from the reactors were controlled and measured by the mass flow controllers. Calibration of the flow capacity was carried out before running the reforming experiments. A thermocouple was inserted into the centre of the catalyst beds to measure the reaction temperature. The products of the bio-oil's steam reforming reactions were analyzed by on-line gas chromatography with a thermal conductivity detector (TCD). Ultra-high purity argon (99.999%) was used as the carrier

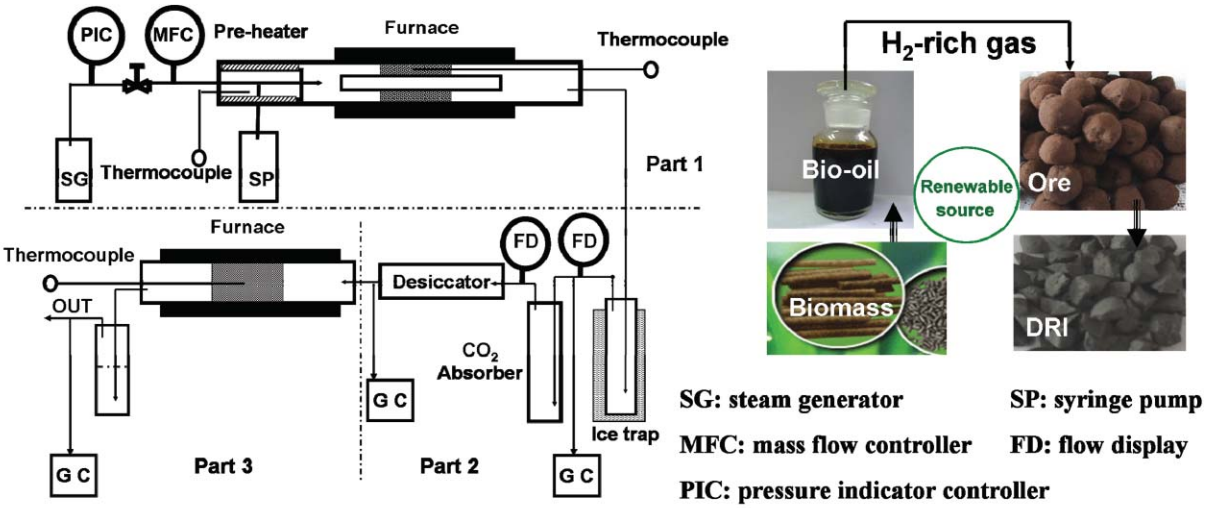

Fig. 10 Schematic diagram of the reaction system for producing DRI based on bio-oil steam reforming gas (left), and the bio-oil-based DRI route using biomass (right).

gas. The reforming products of H_2, CO, CO_2 and CH_4 and other hydrocarbons were detected by GC (column: TDX-01). The composition of the effluent gases from the reactor was also confirmed by a Q-MS mass spectrometer (mode: GSD 300 Omnistar). The reforming performance of the bio-oil was studied by measuring hydrogen yield, carbon conversion and dry gas composition under different reforming conditions. In this work, the hydrogen yield was calculated as a percentage of the stoichiometric potential, in the case of complete conversion of carbon in the bio-oil to CO_2 according to the reaction ($C_nH_mO_k + (2n - k)H_2O = (2n + m/2 - k)H_2 + nCO_2$). The potential yield of hydrogen is $(2n + m/2 - k)$ moles per mole of carbon in the feed. The carbon conversion was calculated by the total moles of carbon in the gaseous products divided by the moles of carbon in the fed bio-oil. In order to produce a high level of reducing gases with a high content of hydrogen, the rich-hydrogen mixture gas from the reforming reactor was further purified by removing CO_2 *via* a 10% sodium hydroxide or sodium carbonate solution in the second unit (Part 2).

The reduction process of the iron oxides in the ores (*i.e.*, producing DRI) occurred in the third unit (Part 3), which was mainly composed of a stainless fixed-bed reactor (named the reduction reactor). The purified reducing gases from Part 2 were fed into the reduction reactor; the flow speed of the gases was controlled and measured by the mass flow controllers. It was externally heated by outside furnaces and the temperature and pressure distribution inside the bed were also precisely monitored. The elemental contents of the resulting DRI products were measured by chemical analysis and X-ray fluorescence analysis performed on SHIMADZU XRF-1800 with Rh radiation. X-Ray diffraction (XRD) measurements were employed to investigate the diffraction structure changes before and after the reduction, which were recorded on an X'pert Pro Philips diffractrometer, using Cu Kα radiation. Generally, all experiments were repeated three times. The difference for each repeat, in general, ranged from 0 to 10%.

Acknowledgements

The authors are grateful to the "National Basic Research Program" (973 Program No. 2007CB210206) of Ministry of Science and Technology of China, the "National High Tech Research and Development Program" (863 Program 2009AA05Z435) and the General Program of the National Natural Science Foundation of China (No. 50772107).

References

1 J. K. Wright, I. F. Taylor and D. K. Philp, *Miner. Eng.*, 1991, **4**, 983–1001.
2 R. J. Fruehan, *Metall. Mater. Trans. B*, 1997, **28**, 743–753.
3 M. Kundak, L. Lazic and J. Crnko, *Metalurgija*, 2009, **48**, 193–197.
4 O. P. Chukwuleke, J. J. Cai, S. Chukwujekwu and S. Xiao, *J. Iron Steel Res. Int.*, 2009, **16**, 1–5.
5 J. Pal, S. Ghosh, M. C. Goswami, D. P. Singh, M. Kumar, R. K. Minj and A. K. Upadhyay, *Steel Res. Int.*, 2007, **78**, 588–594.
6 B. Anameric and S. K. Kawatra, *Miner. Proces. Extr. Metall. Rev.*, 2007, **28**, 59–116.
7 T. Zervas, J. T. McMullan and B. C. Williams, *Int. J. Energy Res.*, 1996, **20**, 157–185.
8 N. A. Warner, *Ironmaking Steelmaking*, 2006, **33**, 277–287.
9 S. Halder and R. J. Fruehan, *Metall. Mater. Trans. B*, 2008, **39**, 784–795.
10 H. Tanaka and T. Harada, *Tetsu To Hagane-J. Iron Steel Inst. Jpn.*, 2006, **92**, 1022–1028.
11 F. Oeters, M. Ottow, A. B. D. Senk, H. B. L. J. GüntnerM. Koltermann, J.-i. Y. A. Buhr, L. Formanek, F. Rose, J. Flickenschild, R. S. R. Hauk, R. Skroch, G. Mayer-Schwinning, H.-L. Bünnagel and H.-G. Hoff, *Iron, Ullmann's Encyclopedia of Industrial Chemistry*, Wiley InterScience, Weinheim, 2009.
12 Y. Ting and S. J. Qing, in *China Non-Blast Furnace Iron-making Conference* Shenyang, 2006.
13 J. Kopfle and R. Hunter, *Ironmaking Steelmaking*, 2008, **35**, 254–259.
14 G. W. Huber, J. W. Shabaker and J. A. Dumesic, *Science*, 2003, **300**, 2075–2077.
15 E. Chornet and S. Czernik, *Nature*, 2002, **418**, 928–929.
16 R. D. Cortright, R. R. Davda and J. A. Dumesic, *Nature*, 2002, **418**, 964–967.
17 R. M. Navarro, M. A. Pena and J. L. G. Fierro, *Chem. Rev.*, 2007, **107**, 3952–3991.
18 J. J. Spivey and A. Egbebi, *Chem. Soc. Rev.*, 2007, **36**, 1514–1528.

19 V. Subramani and S. K. Gangwal, *Energy Fuels*, 2008, **22**, 814–839.
20 W. Lubitz and W. Tumas, *Chem. Rev.*, 2007, **107**, 3900–3903.
21 R. F. Service, *Science*, 2004, **305**, 958–961.
22 J. Bessieres, A. Bessieres and J. J. Heizmann, *Int. J. Hydrogen Energy*, 1980, **5**, 585–595.
23 K. Knop and H. Kubiak, *Stahl Eisen*, 1996, **116**, 55.
24 J. Gretz, W. Korf and R. Lyons, *Int. J. Hydrogen Energy*, 1991, **16**, 691–693.
25 H. Hiebler and J. E. Plaul, *Metalurgija*, 2004, **43**, 155–162.
26 K. H. Tacke and R. Steffen, *Stahl Eisen*, 2004, **124**, 45–52.
27 G. W. Huber, S. Iborra and A. Corma, *Chem. Rev.*, 2006, **106**, 4044–4098.
28 J. G. Seo, M. H. Youn, S. Y. Park, J. S. Chung and I. K. Song, *Int. J. Hydrogen Energy*, 2009, **34**, 3755–3763.
29 F. Melo and N. Morlanes, *Catal. Today*, 2005, **107–108**, 458–466.
30 S. Sato, S. Y. Lin, Y. Suzuki and H. Hatano, *Fuel*, 2003, **82**, 561–567.
31 G. J. Stiegel and M. Ramezan, *Int. J. Coal Geol.*, 2006, **65**, 173–190.
32 D. L. Stojic, M. P. Marceta, S. P. Sovilj and S. S. Miljanic, *J. Power Sources*, 2003, **118**, 315–319.
33 X. Feng, L. Wang and S. L. Min, *Appl. Energy*, 2009, **86**, 1767–1773.
34 C. Okkerse and H. van Bekkum, *Green Chem.*, 1999, **1**, 107–114.
35 M. J. Climent, A. Corma, S. B. A. Hamid, S. Iborra and M. Mifsud, *Green Chem.*, 2006, **8**, 524–532.
36 S. Czernik and A. V. Bridgwater, *Energy Fuels*, 2004, **18**, 590–598.
37 V. Strezov, T. J. Evans and C. Hayman, *Bioresour. Technol.*, 2008, **99**, 8394–8399.
38 A. Corma, S. Iborra and A. Velty, *Chem. Rev.*, 2007, **107**, 2411–2502.
39 P. N. Kechagiopoulos, S. S. Voutetakis, A. A. Lemonidou and I. A. Vasalos, *Energy Fuels*, 2006, **20**, 2155–2163.
40 A. C. Basagiannis and X. E. Verykios, *Catal. Today*, 2007, **127**, 256–264.
41 A. Haryanto, S. Fernando, N. Murali and S. Adhikari, *Energy Fuels*, 2005, **19**, 2098–2106.
42 L. X. Yuan, T. Q. Ye, F. Y. Gong, Q. X. Guo, Y. Torimoto, M. Yamamoto and Q. X. Li, *Energy Fuels*, 2009, **23**, 3103–3112.
43 Y. Q. Chen, L. X. Yuan, T. Q. Ye, S. B. Qiu, X. F. Zhu, Y. Torimoto, M. Yamamoto and Q. X. Li, *Int. J. Hydrogen Energy*, 2009, **34**, 1760–1770.
44 D. N. Wang, S. Czernik and E. Chornet, *Energy Fuels*, 1998, **12**, 19–24.
45 L. Garcia, R. French, S. Czernik and E. Chornet, *Appl. Catal., A*, 2000, **201**, 225–239.
46 C. Rioche, S. Kulkarni, F. C. Meunier, J. P. Breen and R. Burch, *Appl. Catal., B*, 2005, **61**, 130–139.
47 Z. X. Wang, Y. Pan, T. Dong, X. F. Zhu, T. Kan, L. X. Yuan, Y. Torimoto, M. Sadakata and Q. X. Li, *Appl. Catal., A*, 2007, **320**, 24–34.
48 Z. X. Wang, T. Dong, L. X. Yuan, T. Kan, X. F. Zhu, Y. Torimoto, M. Sadakata and Q. X. Li, *Energy Fuels*, 2007, **21**, 2421–2432.
49 L. X. Yuan, Y. Q. Chen, C. F. Song, T. Q. Ye, Q. X. Guo, Q. S. Zhu, Y. Torimoto and Q. X. Li, *Chem. Commun.*, 2008, 5215–5217.
50 *CN. Pat*,., *01263584.7*, 2002.
51 X. Hu and G. X. Lu, *Appl. Catal., B*, 2009, **88**, 376–385.
52 E. C. Vagia and A. A. Lemonidou, *Appl. Catal., A*, 2008, **351**, 111–121.
53 F. R. Feret, *Analyst*, 1998, **123**, 595–600.
54 W. K. Jozwiak, E. Kaczmarek, T. P. Maniecki, W. Ignaczak and W. Maniukiewicz, *Appl. Catal., A*, 2007, **326**, 17–27.
55 A. Brandner, K. Lehnert, A. Bienholz, M. Lucas and P. Claus, *Top. Catal.*, 2009, **52**, 278–287.
56 H. Q. Yang, Z. H. Xu, M. H. Fan, R. Gupta, R. B. Slimane, A. E. Bland and I. Wright, *J. Environ. Sci.*, 2008, **20**, 14–27.
57 C. B. Tarun, E. Croiset, P. L. Douglas, M. Gupta and M. H. M. Chowdhury, *Int. J. Greenhouse Gas Control*, 2007, **1**, 55–61.
58 J. D. Figueroa, T. Fout, S. Plasynski, H. McIlvried and R. D. Srivastava, *Int. J. Greenhouse Gas Control*, 2008, **2**, 9–20.
59 M. R. M. Abu-Zahra, P. H. M. Feron, P. J. Jansens and E. L. V. Goetheer, *Int. J. Hydrogen Energy*, 2009, **34**, 3992–4004.
60 M. T. Ho, G. W. Allinson and D. E. Wiley, *Ind. Eng. Chem. Res.*, 2008, **47**, 4883–4890.

